Delocalization and charge disproportionation in $La_{(1-x)}Sr_xMnO_3$

G. Banach and W. M. Temmerman
Daresbury Laboratory, Daresbury, Warrington WA4 4AD, United Kingdom
(Received 14 August 2003; revised manuscript received 19 November 2003; published 27 February 2004)

Self-interaction corrected local spin-density approximation calculations were performed for $La_{(1-x)}Sr_xMnO_3$ (LSMO) ($0.0<x<0.5$). The influence and inter-relationship of Sr doping, magnetic structure, O displacements, and phase segregation on the Mn charge state were studied. A half-metallic state was obtained for LSMO with manganese configuration Mn^{3+}, whilst Mn^{4+} gave rise to a metallic state with a negligible spin polarization at the Fermi level. Elongating the MnO_6 octahedron led to a Mn^{3+}/Mn^{4+} disproportionation. In the charge disproportionated state the total energy was minimized by an ordered array of Mn^{4+} and Mn^{3+} MnO_2 planes which showed charge ordered stripes.

DOI: 10.1103/PhysRevB.69.054427 PACS number(s): 75.47.−m

I. INTRODUCTION

The half-metallic properties of $La_{(1-x)}Sr_xMnO_3$ ($x=0.3$) (LSMO) are of great importance for applications in spintronics. The tunnel magnetoresistance junction of LSMO/$SrTiO_3$/LSMO shows magnetoresistance ratio in excess of 1800%.[1] This result, according to Ref. 1, strongly underlines the half-metallic nature of mixed-valence manganites. The electronic properties of LSMO, as described by band theory, are nearly half metallic,[2–5] reflecting the so-called transport half-metallic behavior.[6,7] However the fascinating electronic and magnetic properties of LSMO, including colossal magnetoresistance (CMR), indicate that the electronic structure is more complex than the standard band theory picture (see Refs. 8,9). In particular, the electronic structure is determined by the competition of double exchange and superexchange interactions, charge/orbital ordering instabilities, and strong coupling to the lattice deformations. Local Jahn-Teller effects, such as random Jahn-Teller distortions of the MnO_6 (Ref. 10) octahedra, as well as dynamical effects,[11] have recently been invoked to explain the magnetoconductivity and optical conductivity, respectively. Despite the numerous studies of the phase diagram of $LaMnO_3$-$SrMnO_3$ (LMO-SMO) (such as in Refs. 12–14), there are still many conflicting interpretations of the role of the Jahn-Teller effect in this material,[15,16] localization of *d* electrons,[17,18] and polarization of electrons at the Fermi level.[19]

In this paper we discuss issues concerning the charge ordering, and more specifically, the distribution of Mn^{3+} and Mn^{4+} in LSMO. We use the first-principles self-interaction corrected local spin-density (SIC-LSD) approximation.[20] This method can determine the number of valence-band states. Hence, it can differentiate between Mn contributing three states (Mn^{3+}) to the valence band with the remaining four Mn states ($3t_{2g}$ and $1e_g$) localized well below the valence band, and Mn contributing four states (Mn^{4+}) to the valence band, with the remaining three Mn states ($3t_{2g}$) localized below the valence band. This method was successfully applied to the study of orbital order in $LaMnO_3$.[21]

Calculations with the SIC-LSD as a function of Sr doping are presented in this paper for $La_{1-x}Sr_xMnO_3$ where $0.0 \leqslant x \leqslant 0.5$. The Sr doping is modeled with supercells and also with the rigid-band approach. In particular we will be concerned with determining the Mn valency as a function of concentration *x*. It is found, as expected, that the valency changes as a function of Sr doping from Mn^{3+} to Mn^{4+}. However, a mixed phase of Mn^{3+} and Mn^{4+} valencies is found to accompany the valency change. The Mn^{3+}/Mn^{4+} ordering in this mixed phase is consistent with charge-ordered stripes. Furthermore it is found that, in the Mn^{4+} state and as a function of Sr doping, a change of magnetic structure from ferromagnetic to antiferromagnetic takes place. To highlight the effects of Sr doping on the Mn valencies the lattice parameters are kept constant for all concentrations of Sr doping. However, a slightly larger lattice parameter makes the Mn^{3+} valency less unfavorable. Variations in the structural properties of LSMO induce an equally rich variety of charge-ordered states. Elongating the MnO_6 octahedron makes it for the Mn ion more likely to take on the Mn^{3+} valency.

The paper is organized as follows: In the following section we introduce the theoretical background of our electronic structure calculations, and in particular, the self-interaction corrected local spin-density method. The technical and computational details regarding the application of the SIC-LSD to LSMO are discussed in Sec. III. In Sec. IV, we verify that the method works separately for $LaMnO_3$ and $SrMnO_3$. Section V discusses the correlation between magnetic structure and charge order in LSMO. The influence of oxygen displacements on the charge order is investigated in Sec. VI. Section VII presents the results of calculations for various realizations of phase separation and their influence on the charge order. The conclusions of the paper are summarized in Sec. VIII.

II. THEORY

The basis of the SIC-LSD formalism is a self-interaction free total-energy functional E^{SIC} obtained by subtracting from the LSD total-energy functional E^{LSD}, a spurious self-interaction of each occupied electron state ψ_α,[22] namely

$$E^{SIC}=E^{LSD}-\sum_{\alpha}^{occ.}\delta_\alpha^{SIC}. \quad (1)$$

Here α numbers the occupied states and the self-interaction correction for the state α is

$$\delta_{\alpha}^{SIC} = U[n_{\alpha}] + E_{xc}^{LSD}[\overline{n}_{\alpha}], \tag{2}$$

with $U[n_{\alpha}]$ being the Hartree energy and $E_{xc}^{LSD}[\overline{n}_{\alpha}]$ the LSD exchange-correlation energy for the corresponding charge density n_{α} and spin density $\overline{n}_{\alpha}$. The SIC-LSD approach can be viewed as an extension of LSD in the sense that the self-interaction correction is only finite for spatially localized states, while for Bloch-like single-particle states E^{SIC} is equal to E^{LSD}. Thus, the LSD minimum is also a local minimum of E^{SIC}. A question now arises, whether there exist other competitive minima, corresponding to a finite number of localized states, which could benefit from the self-interaction term without losing too much of the energy associated with band formation. This is often the case for rather well localized electrons like the $3d$ electrons in transition metal oxides or the $4f$ electrons in rare-earth compounds. It follows from minimization of Eq. (1) that within the SIC-LSD approach such localized electrons move in a different potential than the delocalized valence electrons which respond to the effective LSD potential. For example, in the case of manganese, three (Mn^{4+}) or four (Mn^{3+}) Mn d electrons move in the SIC potential, while all other electrons feel only the effective LSD potential. Thus, by including an explicit energy contribution for an electron to localize, the *ab initio* SIC-LSD describes both localized and delocalized electrons on an equal footing, leading to a greatly improved description of static Coulomb correlation effects over the LSD approximation.

In order to make the connection between valence and localization more explicit it is useful to define the nominal valence as

$$N_{val} = Z - N_{core} - N_{SIC},$$

where Z is the atomic number (25 for Mn), N_{core} is the number of core (and semicore) electrons (18 for Mn), and N_{SIC} is the number of localized, i.e., self-interaction corrected, states (either three or four for Mn^{4+} and Mn^{3+}, respectively). Thus, in this formulation the valence is equal to the integer number of electrons available for band formation. In this context, nominal valence is closely related to chemical valence. The latter implies, for positive valence, electrons being donated for band filling. To find the valence we assume various atomic configurations, consisting of different numbers of localized states, and minimize the SIC-LSD energy functional of Eq. (1) with respect to the number of localized electrons. The SIC-LSD formalism is governed by the energetics due to the fact that for each orbital the SIC differentiates between the energy gain due to hybridization of an orbital with the valence bands and the energy gain upon its localization. Whichever wins determines if the orbital is part of the valence band or not and in this manner also leads to the evaluation of the valence of elements involved. The SIC depends on the choice of orbitals and its value can differ substantially as a result of this. Therefore, one has to be guided by the energetics in defining the most optimally localized orbitals to determine the absolute energy minimum of the SIC-LSD energy functional. The advantage of the SIC-LSD formalism is that for such systems as transition-metal oxides or rare-earth compounds the lowest-energy solution will describe the situation where some single-electron states may not be Bloch-like. For Mn, these would be the Mn $3d$ states, but not the O $2p$ states, as trying to localize the latter is energetically unfavorable.

In the present work the SIC-LSD approach has been implemented[20] within the linear muffin-tin-orbital (LMTO) atomic sphere approximation (ASA) band structure method,[23] in the tight-binding representation.[24]

III. CALCULATIONAL DETAILS

We performed SIC-LSD calculations for both $La_{(1-x)}Sr_xMnO_3$ for $0.0 < x < 0.5$ and SMO. The space-group symmetry of the LSMO structure changes, as a function of Sr concentration, from $Pnma$ (0% of the Sr) to $R-3c$ (between 10% and ~50% of the Sr) and $P63/mmc$ for SMO. However, for the sake of comparison, we performed calculations using the same cubic crystal structure for all the concentrations. Thus our results for LMO refer to a hypothetical cubic phase. In order to highlight the effect of the electron doping by substituting Sr for La we also kept the lattice parameter constant at 7.32 a.u., which is the average of the theoretical lattice parameters of ferromagnetic LMO and SMO. The experimental lattice parameter, in going from LMO to SMO, changes by 1%, i.e., from 7.45 (Ref. 25) to 7.38 a.u.[26]

For the linear muffin-tin basis functions, we used $6s$, $5p$, $5d$ partial waves for the La and $5s$, $4p$, $4d$ for the Sr atoms, and treated them as low waves.[27] Including also $4f$-basis functions on the lanthanum, treated as intermediate waves, was of no substantial importance for the final results. On the manganese atoms only $4s$ and $3d$ partial waves were treated as low waves, whilst the $4p$ waves were treated as intermediate. On the oxygen only $2s$ and $2p$ partial waves were treated as low waves, and $3d$ waves as intermediate. The atomic sphere radii were 4.0, 2.3, and 1.8 a.u. for the lanthanum and strontium, manganese and oxygen, respectively. These spheres were chosen to minimize the discontinuity in the Hartree potentials, giving an overlap volume of approximately 8%. No empty spheres were used for the cubic system. Care was taken to ensure that the results were converged with respect to both the size of the screening cluster and the number of **k** points for which the one electron equations were solved. This was imperative to allow comparisons to be made between different magnetic structures, which entailed the use of different unit cells. The screening clusters consisting of 111 atoms for the lanthanum, strontium, and manganese sites and 99 atoms for the oxygen atoms were used. The number of **k** points used was 256 in the full Brillouin zone for the paramagnetic/ferromagnetic, G-type and A-type magnetic structures.

To perform calculations for LSMO with $0 < x \leqslant 0.5$, we have utilized the SIC-LSD within the rigid-band model (RBM) and supercell (SC) approach. In the rigid-band model, the variations in the band filling (reduction by up to 0.5 electrons) and lattice constant were the only variables

TABLE I. Energy for different magnetic configurations for cubic $SrMnO_3$ referred to the ground-state energy. The energy differences are per chemical unit cell and the lattice parameter was taken to be 7.32 a.u. The $e_{g(3z^2-r^2)}$ orbital is written as $1e_g$. Also displayed are the magnetic moments (MM) for each of the magnetic structures.

	AF-A		AF-G		FM	
	ΔE [mRy]	MM [μ_B]	ΔE [mRy]	MM [μ_B]	ΔE [mRy]	MM [μ_B]
LSDA	115	2.60	108	2.49	120	2.59
SIC($3t_{2g}$)	5	2.74	0	2.79	12	2.68
SIC($3t_{2g}+1e_g$)	114	3.44	116	3.47	105	3.44

depicting the change from the cubic LMO to LSMO. Thus taking into consideration the dependence on the lattice constant, we could use the results from rigid-band model to describe properties of other perovskites where Sr may be replaced by Ca or Ba. Supercells of the form $La_nSr_mMn_{(n+m)}O_{3(n+m)}$ (where $n=1,\ldots,7$ and $m=1,2,3$) were constructed to describe charge ordering effects due to Mn^{4+} occurring in the vicinity of Sr, and Mn^{3+} present around La sites. Supercells of up to 8 f.u. were used to model the different distributions of Mn^{4+} and Mn^{3+} atoms.

IV. THE END MEMBERS OF PHASE DIAGRAM: LMO AND SMO

We start with the application of the SIC-LSD to the end compounds of LSMO, namely $LaMnO_3$ and $SrMnO_3$. Table I summarizes the LSD and SIC-LSD results for SMO for three different magnetic structures, and two Mn valence configurations. As seen in the table, the Mn^{4+} configuration in the G-type antiferromagnetic (AF-G) structure is the ground-state solution. The latter is insulating, with a band gap of 1.08 eV, twice smaller than the measured band gap[17] of 2.3 eV. The ground-state configuration corresponds to the localization of the three t_{2g} electrons. Localizing an extra d electron, the e_g one with the symmetry $d_{3z^2-r^2}$, giving rise to Mn^{3+}, is unfavorable by more than 100 mRy, for all three different magnetic structures. This energy difference between Mn^{4+} and Mn^{3+} configurations in the ferromagnetic (FM) SMO system decreases from 120 mRy to 93 mRy, when increasing the lattice parameter from 7.2 a.u. (corresponding to the theoretical pseudocubic FM ground state of SMO with Mn^{3+}) to 7.32 a.u. On the other hand, Table I also shows that only 5 mRy separate the G-type from A-type antiferromagnetic (AF-A) state. This shows that the charge-ordering energy in SMO is a much larger energy scale than the magnetic order and that its dependence on the lattice constant is small.

The FM cubic $LaMnO_3$ with the lattice parameter of 7.43 a.u. has the Mn^{3+} configuration: 15 mRy separate this ground state from the Mn^{4+} excited state. In comparison, for the Jahn-Teller distorted $LaMnO_3$ structure, we find 20 mRy energy difference.[21] Reducing the lattice constant by 1.5% to 7.32 a.u., we find that $LaMnO_3$ becomes nearly tetravalent and less than 5 mRy separate the Mn^{3+} ground state from the Mn^{4+} excited state. We find the crossover between trivalent and tetravalent manganese at a volume of elementary cell equal to 215 Å^3. This is close to the expected volume of 210 Å^3 from pressure experiments.[28] The calculations show that the energy scales between the Mn^{3+} and Mn^{4+} charge-ordered state are much smaller for LMO than for SMO, specifically 20 times smaller. Actually, this is an energy scale comparable to the energy difference between magnetic structures. The competition between these energy scales in the

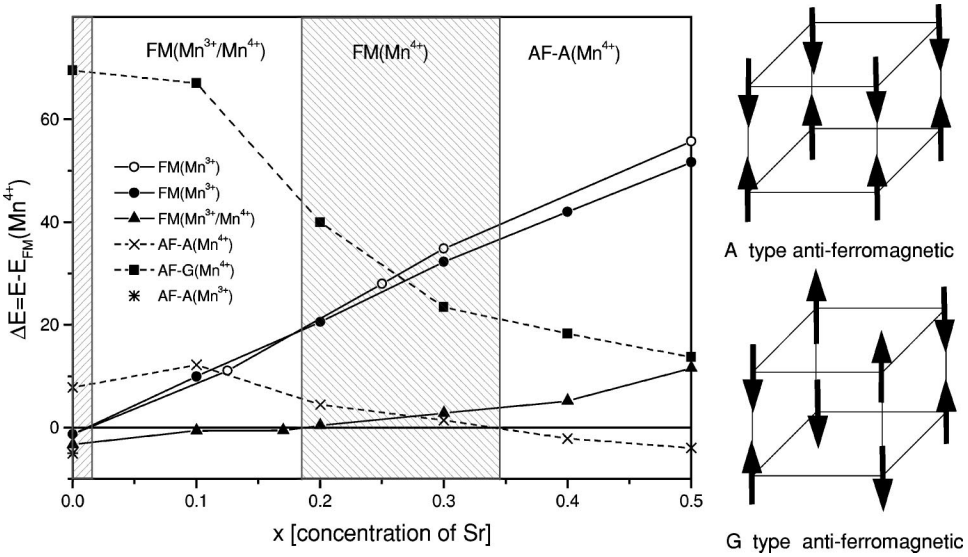

FIG. 1. Left: Energy phase diagram LMO-LSMO in the cubic structure with the lattice constant of 7.32 a.u. The energy for all the systems is with respect to the energy of FM system with Mn^{4+}. For Sr concentrations up to 20% FM(Mn^{3+}/Mn^{4+}) is the state with the lowest energy. Sr concentrations in excess of 20% find FM(Mn^{4+}) to be the state with the lowest energy and beyond Sr concentrations of 35% the magnetic structure changes to AF-A. The full line with open (full) circles marks the supercell (rigid-band model) results for FM(Mn^{3+}). Right: Schematic views of the AF-A and AF-G structures.

TABLE II. Energy for three different magnetic configurations with reference to ground-state energy for cubic $La_{0.5}Sr_{0.5}MnO_3$. Energy differences are per chemical unit cell and the lattice parameter was taken to be 7.32 a.u. ΔE_{RBM} refers to the energy difference from a RBM, whilst ΔE_{SC} is the energy difference obtained using a SC model ($LaSrMn_2O_6$). The symbol MM stands for magnetic moment. Four different valence configurations are considered: LSDA, Mn^{4+} with the three t_{2g} electrons localized and the two Mn^{3+} valence configurations, localizing each of the e_g separately.

	ΔE_{RBM} [mRy]	MM [μ_B]	ΔE_{SC} [mRy]	MM [μ_B]
AF-A				
LSDA	113	2.67	108	2.77
SIC($3t_{2g}$)	0	3.04	0	2.99
SIC($3t_{2g}+e_{g(3z^2-r^2)}$)	63	3.51	63	3.51
SIC($3t_{2g}+e_{g(x^2-y^2)}$)	48	3.53	47	3.53
AF-G				
LSDA	120	2.62	122	2.56
SIC($3t_{2g}$)	18	3.02	22	2.89
SIC($3t_{2g}+e_{g(3z^2-r^2)}$)	64	3.50	62	3.50
SIC($3t_{2g}+e_{g(x^2-y^2)}$)	64	3.50	63	3.50
FM				
LSDA	111	2.69	113	2.70
SIC($3t_{2g}$)	4	2.91	6	2.86
SIC($3t_{2g}+e_{g(3z^2-r^2)}$)	56	3.51	57	3.50
SIC($3t_{2g}+e_{g(x^2-y^2)}$)	52	3.52	54	3.52

case of Sr doping will be the subject of the next three sections.

V. MAGNETIC STRUCTURE AND CHARGE ORDER IN LSMO

In Fig. 1 we present the phase diagram of antiferromagnetically and ferromagnetically ordered LSMO for Sr concentration between 0.0 and 0.5. For LMO, we obtain a ground state of Mn^{3+} valency in an AF-A magnetic structure. In the range of x up to approximately 0.2 (excluding 0.0), the FM supercell with Mn^{3+} and Mn^{4+} disproportionation gives the state with the lowest energy. A crossover, as a function of Sr doping, from a FM Mn^{3+} and Mn^{4+} disproportionated ground state to a FM Mn^{4+} ground state occurs around 20% Sr doping. For Sr concentrations between $\sim$20% and $\sim$35% the ground state has the valency of Mn^{4+} in a ferromagnetic structure. For Sr concentrations larger than $\sim$35%, the magnetic structure changes to AF-A, but the valency remains Mn^{4+}. From Fig. 1, we note that the larger the hole doping becomes the more unfavorable the Mn^{3+} configuration turns out to be. We find that the disproportionation into Mn^{3+} and Mn^{4+} is dependent on Sr concentration: more Mn^{3+} are present for lower Sr concentrations and by $\sim$20% of Sr all Mn^{3+} is gone.

The $La_{0.5}Sr_{0.5}MnO_3$ system was studied using both the rigid-band model and $LaSrMn_2O_6$ supercell. From Table II, we note that in the LSD we obtain a FM state in the rigid-band model, whilst an AF-A state is obtained in the supercell

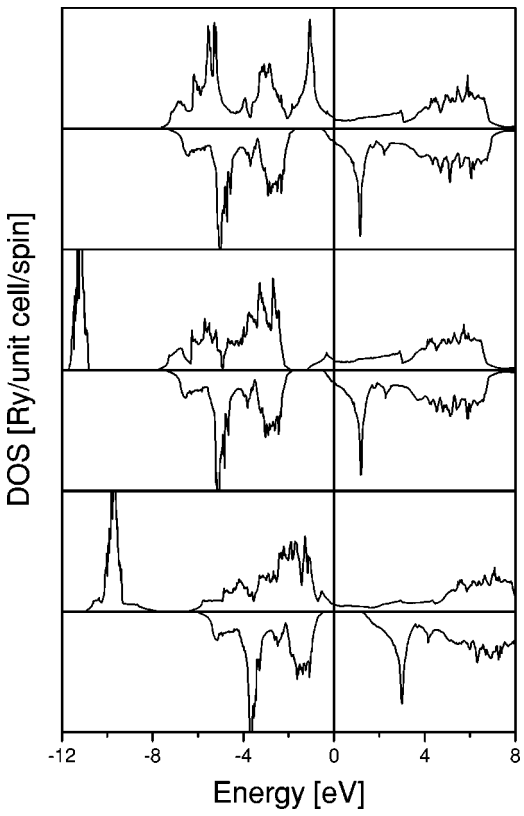

FIG. 2. Density of states for FM $La_{.7}Sr_{.3}MnO_3$ from rigid-band model for minority and majority spin channels with respect to the Fermi energy. Displayed are: LSD calculation (top), SIC-LSD calculation for the ground state of three localized t_{2g} electrons (center) and SIC-LSD calculation for four localized electrons ($3t_{2g}+e_{g(3z^2-r^2)}$) (bottom).

approximation. The SIC-LSD calculations give the same ground state both in the rigid-band model and supercell. Small energy differences of 4 and 6 mRy separate the AF-A ground state from the FM state in the rigid-band model and supercell, respectively. Figure 1 also confirms that the rigid-band model is an adequate description of the disordered La/Sr system. A comparison is made with supercell calculations of $La_nSrMn_{(n+1)}O_{3(n+1)}$ with $n=1,\ldots,7$ for the FM Mn^{3+} configuration. From Table II, we note that the energy differences between Mn^{4+} and Mn^{3+} are more or less constant with respect to the magnetic structure and also with respect to the symmetry of the localized e_g electron in the Mn^{3+} configuration. This energy is approximately 60 mRy and the energy differences between magnetic structures are an order of magnitude lower.

The energies in Fig. 1 are closely balanced and changes in the lattice constant can alter the state with the lowest energy. Increasing the lattice constant by 1% to 7.39 a.u., we find that the Mn^{3+} configuration has become slightly less unfavorable. This we note, for example, by comparing the energy difference for $La_{0.7}Sr_{0.3}MnO_3$ between FM Mn^{4+} and Mn^{3+} configurations which reduces from 32 mRy at lattice constant 7.32 a.u. to 21 mRy at the 1% increased lattice constant of 7.39 a.u. For $La_{0.5}Sr_{0.5}MnO_3$ even the ground state changes from AF-A at the lattice constant of 7.32 a.u. to FM at 7.39

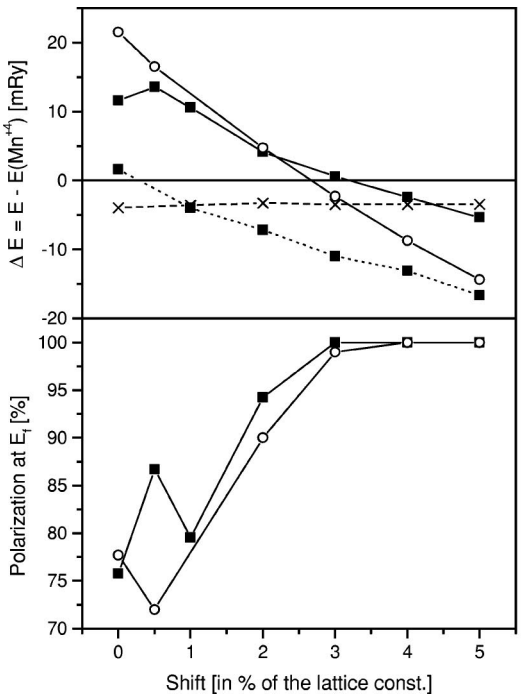

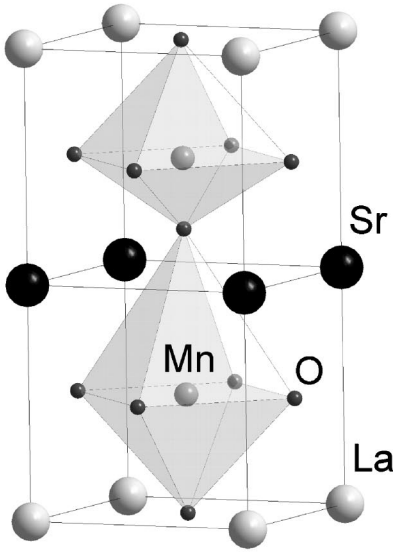

FIG. 3. Left: In the top panel the energy difference for the FM system in the Mn^{4+}/Mn^{3+} mixed valence state: squares with solid line—rigid-band model (for $x=0.5$); open circles—supercell model ($LaSrMn_2O_6$); squares with dotted line—rigid-band model (for $x=0.3$), crosses with dashed line AF-A with Mn^{4+} (for $x=0.5$). All energies are with respect to the energy of the FM system with Mn^{4+}. In the bottom panel: polarization of electrons at the Fermi level: squares—from rigid-band model (for $x=0.5$) and open circles for supercell model ($LaSrMn_2O_6$). Right: Schematic view of the unit cell.

a.u. This shows that the combined effect of band filling and the value of the lattice constant gives rise to a rich variation in magnetic structure and charge order.

The spin magnetic moments increase only slightly in comparison with LSD results. For $La_{0.7}Sr_{0.3}MnO_3$ the Mn spin magnetic moment is 3.14 μ_B in SIC-LSD and 3.03 μ_B in LSD and for $La_{0.5}Sr_{0.5}MnO_3$ these are 2.91 μ_B and 2.69 μ_B, respectively. The density of states for LSD calculations and the SIC-LSD in Mn^{4+} and Mn^{3+} configurations are shown in Fig. 2. We clearly see the majority Mn t_{2g} peak, which occurs in the LSD calculation just below the Fermi level, which moves down in energy below the bottom of the valence band for the calculations for Mn^{4+} and Mn^{3+} valencies. In the Mn^{4+} ground-state configuration for $La_{0.7}Sr_{0.3}MnO_3$ a metallic state is obtained and the electronic structure in the vicinity of the Fermi level is similar to the LSD, i.e., it is also a nearly half-metallic system. However, for the Mn^{3+} configuration, we obtain a half metal with 1.6 eV band gap in the majority spin channel. We will see in the following that the occurrence of a half-metallic density of states is closely associated with the Mn^{3+} valency.

VI. OXYGEN DISPLACEMENTS AND CHARGE ORDER IN LSMO

We investigated the influence, on the Mn valency, of a tetragonal shift of the oxygen atom. We calculated the total energies for a double unit cell for each combination of configurations Mn^{3+} and Mn^{4+}. In the top of Fig. 3 we show the total energies of AF-A with Mn^{4+} and FM with mixed valence Mn^{3+}/Mn^{4+} configuration as a function of tetragonal shift of O atom. In the latter case the Mn^{3+} atom is taken to be inside the octahedron which is elongated by the tetragonal shift (see the cell on the right-hand side of Fig. 3). This is the most favorable scenario; placing the Mn^{4+} and the Mn^{3+} in the reverse order was the most unfavorable scenario. For $La_{0.5}Sr_{0.5}MnO_3$ the disproportionated Mn^{4+}/Mn^{3+} ground state occurs at 4% shift in the rigid-band model and a 3% shift in the supercell model. The crossover to a new ground state depends on the Sr concentration and for $La_{0.7}Sr_{0.3}MnO_3$ we find the new ground state already at an 1% upward shift of O. Additionally, for shifts larger than 3% of the lattice constant the system becomes fully polarized at the Fermi level (in the bottom panel of Fig. 3) and we obtain a half-metallic state. In Fig. 4 we show the density of states for the disproportionated Mn^{4+}/Mn^{3+} system without tetragonal shift, with tetragonal shift for oxygen atom (4% of lattice constant) and for AF-A system with Mn^{4+} configuration. This system becomes half metallic with a band gap in one spin channel equal to 0.48 eV. The magnetic moment on Mn^{3+} increases slightly by 0.11 μ_B and decreases about 0.18 μ_B on Mn^{4+}. The oxygen atom, shifted in the supercell calculation, has a magnetic moment twice larger than in the undistorted structure.

In Fig. 5 we present a different tetragonal displacement involving two symmetrical shifts of 5% of the lattice parameter for two oxygen atoms from LaO and SrO layers in $La_2SrMn_3O_9$. For the disproportionated ground-state configuration of $Mn^{3+}/Mn^{4+}/Mn^{3+}$ we obtain a half-metallic state. In comparison with the above Mn^{4+}/Mn^{3+} double unit cell, the band gap has become nearly twice larger at 0.8 eV. This is due to the higher concentration of Mn^{3+} atoms in the latter supercell. The results of these two implementations of tetragonal distortions show that if random Jahn-Teller distortions occur,[15] the system can become locally half metallic.

VII. PHASE SEPARATION AND CHARGE ORDER IN LSMO

Supercells in the FM regime were also constructed to model both the influence of Mn^{4+} and Mn^{3+} ordering on the

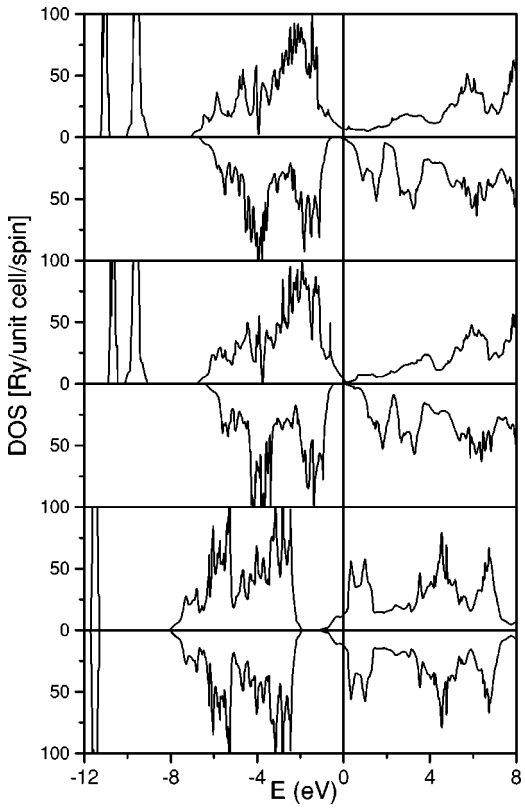

FIG. 4. DOS for $LaSrMn_2O_6$ with mixed valence Mn^{4+}/Mn^{3+} configurations for minority and majority spin channel; is metallic without tetragonal shift for oxygen atom (top); is half metallic with a tetragonal shift applied to the oxygen atom of 0.04 of the lattice constant (center). In the bottom panel is the DOS for the antiferromagnetic ground state of Mn^{4+} without tetragonal shift.

total energy and the influence of the ordering of the LaO and SrO planes on the Mn charge order. Specifically, supercells of the form $La_nSrMn_{(n+1)}O_{3(n+1)}$ with $n=2,\ldots,7$ and $La_4Sr_2Mn_6O_{18}$, and $La_4Sr_4Mn_8O_{24}$ were studied. Calculations for these systems were in agreement with the results of Fig. 1. Specifically, for n smaller than 4, the $La_nSrMn_{(n+1)}O_{3(n+1)}$ systems had an Mn^{4+} ground state and for n larger than 4, the mixed valence Mn^{4+}/Mn^{3+} system became the ground state.

TABLE III. Total energy differences (in meV), with respect to the state with the lowest energy, for different distributions of manganese ions, in six units supercell in the rigid band (corresponding to $La_{0.83}Sr_{0.17}MnO_3$) and in the supercell $La_5SrMn_6O_{18}$. For $La_5SrMn_6O_{18}$ the system is ordered as SrO-LaO-LaO-LaO-LaO-LaO and the Mn^{4+} or Mn^{3+} ions are sandwiched in between.

Scenario	Supercell	Rigid band model
444444	27	7
444443	36	–
444434	34	7
444344	48	–
443344	54	41
444343	27	11
434434	45	18
434343	0	0
444333	79	63
334433	104	102
334343	59	52
343343	45	43
333333	213	215

For the mixed-valence configuration, we investigated the influence of different distributions of Mn^{4+} and Mn^{3+} on the total energy. In particular, we studied different scenarios of distributions of Mn^{4+}/Mn^{3+} atoms from all Mn^{4+} (denoted by 444444 in Table III) to all Mn^{3+} (referred to as 333333 in Table III), using both a six chemical units rigid-band model of $La_{0.83}Sr_{0.17}MnO_3$ and the $La_5SrMn_6O_{18}$ supercell. In the supercell, the SrO layer was taken to be at the bottom of the cell. The energy differences are small and to emphasize this we write them down in meV. They are nearly equal to the magnitude of magnetic structure energy differences. The distribution 434343 of Mn^{4+} and Mn^{3+} valencies was the most favorable energy state at 17% Sr concentration for both the

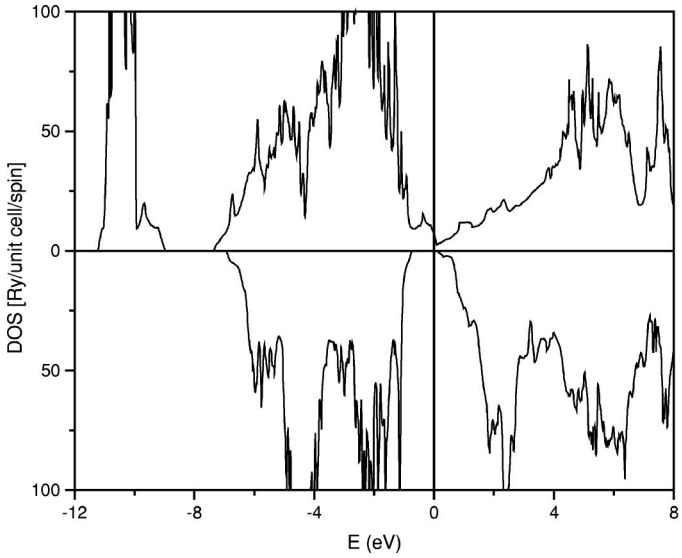

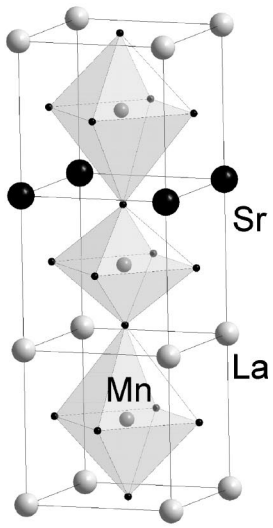

FIG. 5. Left: DOS, in minority and majority spin channels, for $La_2SrMn_3O_9$ with symmetrically shifted (by 0.05 of lattice constant) oxygen atoms for the mixed $Mn^{3+}/Mn^{4+}/Mn^{3+}$ configuration. Right: Schematic view of the unit cell.

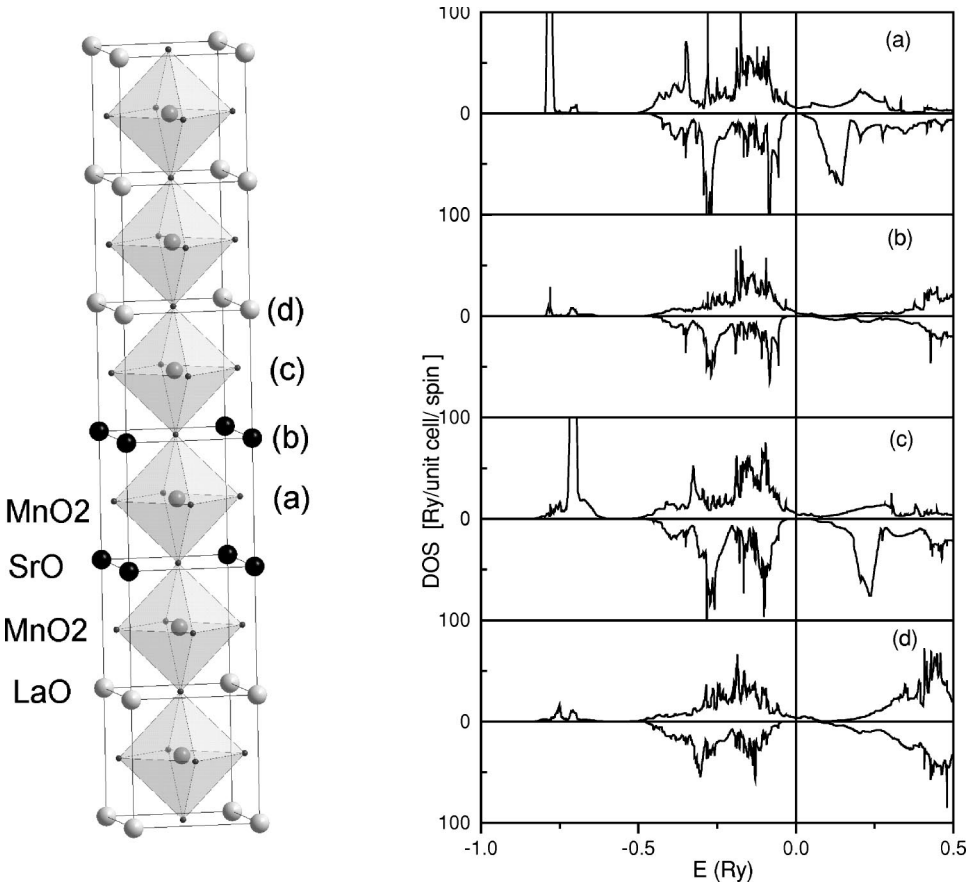

FIG. 6. Local DOS for a supercell $La_4Sr_2Mn_6O_{18}$ (right). The configuration is (a) one MnO_2 layer of Mn^{4+} sandwiched between the SrO layers (marked as black balls) and Mn^{3+} in all other MnO_2 planes. Here (b) refers to SrO plane, (c) to MnO_2 plane, and (d) to LaO plane. The left-hand side picture shows the structure.

supercell and the rigid-band model calculations. A different distribution of the same amount of Mn^{4+} and Mn^{3+} atoms denoted by 444333 is about as unfavorable as localizing an extra Mn *d* electron, as realized in 334433 scenario, or delocalizing an Mn *d* electron as it happens in 443344 scenario. The energy differences between rigid-band model calculations and the supercell show that SrO and LaO layers do matter. In the rigid-band model we see smaller energy differences upon increasing the amount of Mn^{4+} cations (only 7 meV separate the 444444 state from the ground state) than upon decreasing the amount of Mn^{4+} cations (215 meV separate the 333333 state from the ground state). In the supercell approach this trend is not as pronounced and whilst 213 meV separate the 333333 state from the ground state, the 444444 configuration is further away from the ground state, by 27 meV, than in the rigid-band model.

The $La_4Sr_2Mn_6O_{18}$ system, i.e., increasing the Sr concentration to $\sim$30%, acquires the Mn^{4+} ground-state configuration and is metallic. For this system we have studied the influence of the distribution of SrO and LaO layers on the total energy. The state with the lowest energy was attained by phase separating the SrO layers from the LaO layers, namely, the two SrO layers were nearest neighbors. Separating the two SrO layers by one and two LaO layers, respectively, increases respectively the energy of the system by 2 and 5 mRy.

In Fig. 6, we show density of states (DOS) of one of the configurations of $La_4Sr_2Mn_6O_{18}$. The configuration is such that we have one MnO_2 plane with Mn^{4+}, sandwiched between two SrO planes, and all other MnO_2 planes are occupied by Mn^{3+}. This supercell can be considered as a model of phase separated LSMO which was studied by Koida.[29] It is also of relevance to the $La_{0.7}Ca_{0.3}MnO_3$ system investigated by Bibes.[30] As can be seen from Fig. 6, this system LSMO is half metallic. Energetically unfavorable, however, the energy difference between this state and the ground state is reduced to 20 mRy, in comparison with the energy difference between all Mn having the Mn^{3+} configuration and the ground state (33 mRy). The gap is reduced from 0.68 eV (the scenario with the configuration of Mn^{3+} for all manganese atoms) to 0.54 eV. Note that this pseudogap is constant for all MnO_2 layers, independently of their valence. None of the supercells had this Mn^{3+} valence in their ground-state configuration. However one could speculate that maybe at the surface Mn^{3+} could be the stable configuration since the lower coordination would favor the more localized state. More complex supercells, where more Sr layers could phase separate, could plausibly lead to a half-metallic ground state.

VIII. CONCLUSIONS

We have found that upon Sr doping the Mn^{3+} valency of LMO becomes more and more unfavorable with respect to the Mn^{4+} valence. Reducing the carrier concentration upon Sr doping makes it energetically unfavorable to localize four Mn *d* states and one of these localized states delocalizes, leading to a nominal valency of Mn^{4+}. For Sr concentrations less than 20%, a disproportionated Mn^{4+}/Mn^{3+} ground state

was obtained, whilst for concentrations in excess of 20% a Mn^{4+} ground state was obtained. Also, a close competition between FM and AF-A Mn^{4+} states was seen with a crossover from FM to AF-A Mn^{4+} around 35% Sr concentration. The Mn^{4+} ground state, for concentrations larger the 20% Sr, has marginal spin polarization at the Fermi level. We found, however, that the Mn^{3+} valency was not that energetically unfavorable and that small increases in the lattice parameter would lead to the occurrence of Mn^{3+} in a mixed valence Mn^{4+}/Mn^{3+} state. Likewise, elongations of the MnO_6 octahedra lead to the formation of Mn^{3+} valence atoms. With the appearance of Mn^{3+} ions a half-metallic state is obtained. Furthermore, in the disproportionated Mn^{4+}/Mn^{3+} state we found that the total energy is minimized by an ordered array of Mn^{4+} and Mn^{3+} MnO_2 planes. The relation of this finding to the observed charge-ordered stripes[31] will be the topic of a further study.

As the Sr doping increases, the Mn^{4+} state becomes more and more favored with respect to the Mn^{3+}. The Sr doping results in one more valence-band electron which is obtained from delocalizing a Mn^{3+} e_g state. In other words, Sr hole doping favors band formation instead of localization.

For $La_{0.7}Sr_{0.3}MnO_3$, of huge relevance to spintronics applications, we suggest the following scenario to explain the half-metallic properties. Whilst in $La_{0.7}Sr_{0.3}MnO_3$, from x-ray results, every Mn-O bondlength is the same at 1.949 Å,[32] the bondlengths of Mn-O in distorted LMO change from 1.907 to 2.179 Å, depending on direction. It seems however, based on pulsed-neutron-diffraction measurements,[15] that the Jahn-Teller distortion is still present in LSMO and could therefore, according to our analysis, lead to the formation of Mn^{3+} ions, which would be sufficient to give rise to a half-metallic state. Therefore, our results indicate that half metallicity could already be present in the density of states.

In conclusion, it seems that the competition between Mn^{3+} and Mn^{4+} for Sr concentrations below 50% provides a useful framework for the understanding of the rich variety in the electronic and magnetic properties of LSMO.

ACKNOWLEDGMENTS

G.B. was supported by the EU-funded Research Training Network: ''Computational Magnetoelectronics'' (Grant No. HPRN-CT-2000-00143). He also gratefully acknowledges discussions with Dr. A. Haznar and Dr. R. Tyer.

[1] M. Bowen, M. Bibes, A. Barthelemy, J.-P. Contour, A. Anane, Y. Lemaitre, and A. Fert, Appl. Phys. Lett. **82**, 233 (2003).
[2] W.E. Pickett and D.J. Singh, J. Magn. Magn. Mater. **172**, 237 (1997).
[3] D.J. Singh and W.E. Pickett, Phys. Rev. B **57**, 88 (1998).
[4] D.J. Singh and W.E. Pickett, J. Appl. Phys. **83**, 7354 (1998).
[5] E.A. Livesay, R.N. West, S.B. Dugdale, G. Santi, and T. Jarlborg, J. Phys.: Condens. Matter **11**, L2711 (1999).
[6] B. Nadgorny, I.I. Mazin, M. Osofsky, R.J. Soulen, Jr., P. Broussard, R.M. Stroud, D.J. Singh, V.G. Harris, A. Arsenov, and Y. Mukovskii, Phys. Rev. B **63**, 184433 (2001).
[7] I.I. Mazin, Phys. Rev. Lett. **83**, 1427 (1999).
[8] J.M.D. Coey and M. Viret, Adv. Phys. **48**, 167 (1999).
[9] Y. Tokura and Y. Tamioka, J. Magn. Magn. Mater. **200**, 1 (1999).
[10] M. Dzero, L.P. Gor'kov, and V.Z. Kresin, J. Mol. Struct. **17**, 2095 (2003).
[11] B. Michaelis and A.J. Millis, Phys. Rev. B **68**, 115111 (2003).
[12] J. Hemberger, A. Krimmel, T. Kurz, H.-A. Krug von Nidda, V.Yu. Ivanov, A.A. Mukhin, A.M. Balbashov, and A. Loidl, Phys. Rev. B **66**, 094410 (2002).
[13] Ryo Maezono, Sumio Ishihara, and Naoto Nagaosa, Phys. Rev. B **58**, 11 583 (1998).
[14] Peter Majewski, Lars Epple, Michael Rozumek, Heike Schluckwerder, and Fritz Aldinger, J. Mater. Res. **15**, 1161 (2000).
[15] Despina Louca and T. Egami, Phys. Rev. B **59**, 6193 (1999).
[16] J.L. Cohn, J.J. Neumeier, C.P. Popoviciu, K.J. McClellan, and Th. Leventouri, Phys. Rev. B **56**, R8495 (1997).
[17] T. Saitoh, A.E. Bocquet, T. Mizokawa, H. Namatame, A. Fujimori, M. Abbate, Y. Takeda, and M. Takano, Phys. Rev. B **51**, 13 942 (1995).
[18] G. Subias, J. Garcia, M.G. Proietti, and J. Blasco, Phys. Rev. B **56**, 8183 (1997).
[19] J.-H. Park, E. Vescovo, H.-J. Kim, C. Kwon, R. Ramesh, and T. Venkatesan, Nature (London) **392**, 794 (1998).
[20] W. M. Temmerman, A. Svane, Z. Szotek, and H. Winter, in *Electronic Density Functional Theory: Recent Progress and New Directions*, edited by J. F. Dobson, G. Vignale, and M. P. Das (Plenum Press, New York, 1998).
[21] R. Tyer, W.M. Temmerman, Z. Szotek, G. Banach, A. Svane, L. Petit, and G.A. Gehring, cond-mat/0303602 (unpublished).
[22] J.P. Perdew and A. Zunger, Phys. Rev. B **23**, 5048 (1981).
[23] O.K. Andersen, Phys. Rev. B **12**, 3060 (1975).
[24] O.K. Andersen and O. Jepsen, Phys. Rev. Lett. **53**, 2571 (1984).
[25] B.C. Haubak, H. Fjelvag, and N. Sakai, J. Solid State Chem. **124**, 43 (1996).
[26] P.D. Baattle, T.C. Gibb, and C.W. Jones, J. Solid State Chem. **74**, 60 (1988).
[27] W.R.L. Lambrecht and O.K. Andersen, Phys. Rev. B **34**, 2439 (1986).
[28] I. Loa, P. Adler, A. Grzechnik, K. Syassen, U. Schwarz, M. Hanfland, G.Kh. Rozenberg, P. Gorodetsky, and M.P. Pasternak, Phys. Rev. Lett. **87**, 125501 (2001).
[29] T. Koida, M. Lippmaa, T. Fukumura, K. Itaka, Y. Matsumoto, M. Kawasaki, and H. Koinuma, Phys. Rev. B **66**, 144418 (2000).
[30] M. Bibes, Ll. Balcells, S. Valencia, J. Fontcuberta, M. Wojcik, E. Jedryka, and S. Nadolski, Phys. Rev. Lett. **87**, 067210 (2001).
[31] P. Littlewood, Nature (London) **399**, 529 (1999).
[32] S.J. Hibble, S.P. Cooper, A.C. Hannon, I.D. Fawcett, and M. Greenblatt, J. Phys.: Condens. Matter **11**, 9221 (1999).